

# Continuous-Wave Optically Pumped 1.55 $\mu\text{m}$ InAs/InAlGaAs Quantum Dot Microdisk Lasers Epitaxially Grown on Silicon

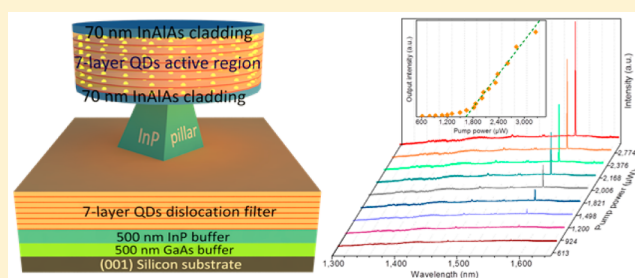
Bei Shi,<sup>†</sup> Si Zhu,<sup>†</sup> Qiang Li,<sup>†</sup> Yating Wan,<sup>†</sup> Evelyn L. Hu,<sup>‡</sup> and Kei May Lau<sup>\*,†</sup>

<sup>†</sup>Department of Electronic and Computer Engineering, Hong Kong University of Science and Technology, Clear Water Bay, Kowloon, Hong Kong

<sup>‡</sup>School of Engineering and Applied Sciences, Harvard University, Cambridge, Massachusetts 02138, United States

**ABSTRACT:** Monolithic integration of high-performance semiconductor lasers on silicon enables wafer-scale optical interconnects within photonic integrated circuits on a silicon manufacturing platform. III–V quantum dot (QD) lasers on silicon stand out for their better device performances and reliability. QD lasers grown on III–V substrates have been integrated by wafer-bonding techniques with high quality. Direct growth of QD lasers on silicon offers an alluring alternative, using widely available large-area silicon substrates. However, to date, notable achievements have been reported only in InAs/GaAs lasers emitting at 1.3  $\mu\text{m}$ , while 1.55  $\mu\text{m}$  InAs/InP QD lasers on silicon remain in uncharted territory. Here we demonstrate the first 1.55  $\mu\text{m}$  band InAs/InAlGaAs quantum dot microdisk lasers epitaxially grown on (001) silicon substrates. The lasing threshold for the seven-layer quantum dot microdisk laser at liquid-helium temperature is 1.6 mW under continuous optical pumping. The observed lasing is attributed to a unique combination of the high-quality QDs, small mode volume, and smooth sidewall of the microdisk structure and a well-developed InP buffer incorporating quantum dots as dislocation filters. These results thus mark a major step toward an integrated III–V-on-silicon photonics platform.

**KEYWORDS:** monolithic integration, microdisk lasers, quantum dots, direct epitaxy, III–V on silicon



On-chip optical interconnects promise to outperform electrical links, with high-bit rate and large-capacity data communications,<sup>1</sup> which are key drivers for the recent surge of silicon photonics development. While group IV photonics have leveraged high-quality SiGe/Ge on silicon to demonstrate photodetectors,<sup>2</sup> modulators,<sup>3</sup> resonators,<sup>4</sup> and waveguides,<sup>5</sup> highly efficient, high-performance viable lasers on silicon remain challenging.<sup>6,7</sup> Taking advantage of the direct band gap nature of III–V semiconductors, various hybrid III–V lasers on silicon realized by bonding techniques have shown impressive performance.<sup>8–12</sup> In addition to the immediate advantage of low-cost, large-area, robust, and high-quality silicon substrates, direct epitaxial growth of III–V lasers on silicon represents a desirable alternative toward eventual monolithic integration of photonics and electronics. Future specific photonic integrated circuit (PIC) designs can be realized and made compatible with foundry technologies offering tight tolerance. Nevertheless, this approach faces serious challenges associated with the lattice and thermal mismatch as well as the different polarity between III–V materials and silicon.<sup>13</sup> Recently, remarkable progress has been made toward high-performance InAs/GaAs quantum dot (QD) lasers grown on silicon substrates. J. Yang et al. reported In<sub>0.5</sub>Ga<sub>0.5</sub>As/GaAs QD lasers on silicon emitting at  $\sim 1 \mu\text{m}$ , with multiple-layer QD dislocation filters.<sup>14</sup> H. Liu et al. first demonstrated 1.3  $\mu\text{m}$  QD lasers on silicon under room-

temperature (RT) pulsed conditions using an InAs/InGaAs dot-in-a-well (DWELL) structure.<sup>15</sup> Later, A. Y. Liu et al. successfully realized a high-performance RT continuous-wave (CW) QD laser on Ge-buffered silicon with 6° miscut toward the [111] plane to surpass antiphase domains (APDs).<sup>16</sup> Ridge waveguide lasers with thresholds as low as 430 A/cm<sup>2</sup>, output power exceeding 176 mW, and lasing up to 119 °C were fabricated. In addition to the electrically injected lasers, optically pumped QD microdisk lasers have also been demonstrated on on-axis (001) silicon by Y. Wan et al. The lasing thresholds were comparable with the same structure grown on GaAs substrates, taking advantage of the V-grooved Si substrates.<sup>17</sup> Besides the good device performances, the reliability of QD lasers on silicon has also been significantly improved with respectable operating lifetimes over thousands of hours.<sup>18,19</sup> However, so far, the emission wavelengths of all the QD lasers grown on silicon have been limited at 1.3  $\mu\text{m}$  or less. A highly efficient III–V laser on silicon operating in the 1.55  $\mu\text{m}$  band for inter/intrachip optical interconnect is still lacking.<sup>20,21</sup> QD lasers in this wavelength range are generally built on InP-based material systems and grown on lattice-matched InP substrates to provide high-quality 1.55  $\mu\text{m}$  emission.<sup>22</sup> A technology that allows the formation of such

Received: September 25, 2016

Published: January 9, 2017

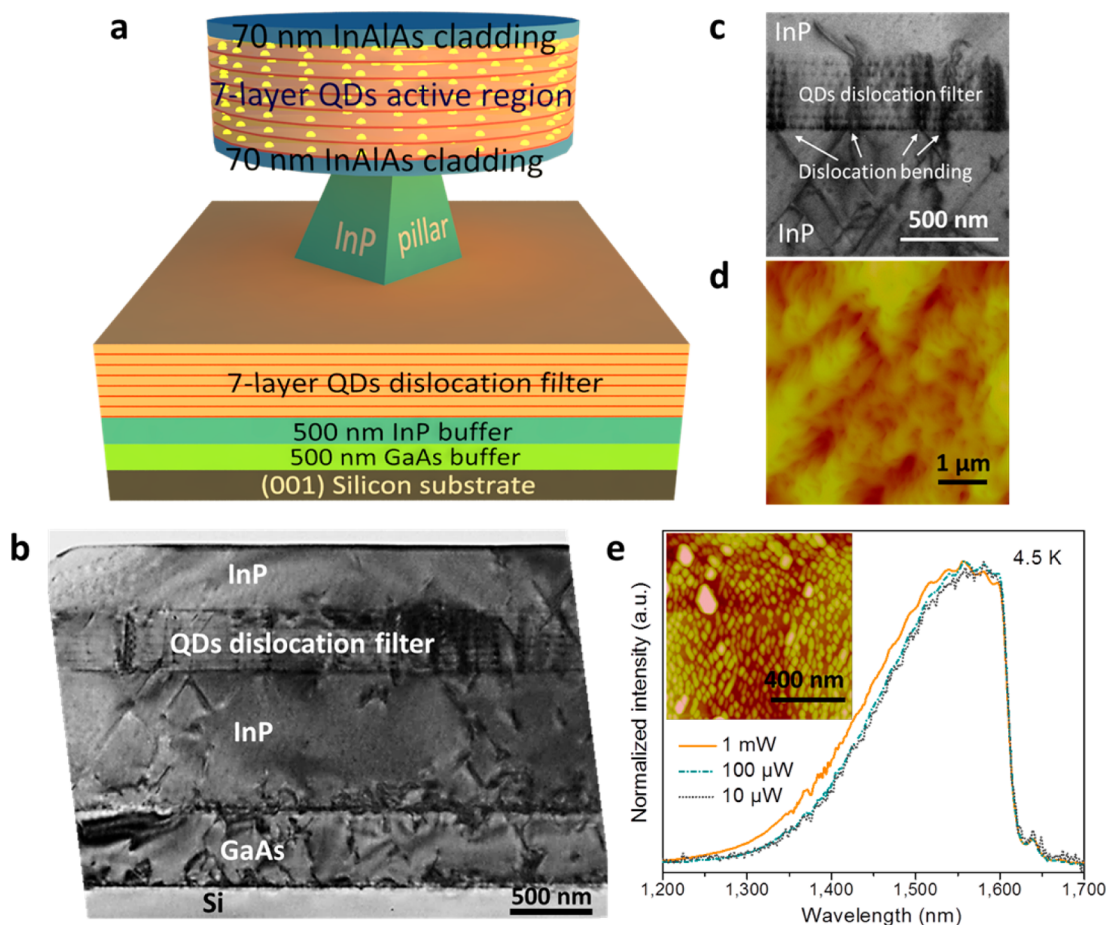


**Figure 1.** Epitaxial structure and characterization of an as-grown QD microdisk on Si. (a) Schematic diagram of the fabricated microdisk laser epilayer structure. (b) Cross-sectional TEM images demonstrating the top InP buffer with reduced dislocations and (c) the dislocation filtering mechanism. (d)  $5 \times 5 \mu\text{m}^2$  AFM image of the InP-on-Si with an RMS value of 3.1 nm; the color scale is 40 nm. (e) Power-dependent photoluminescence spectra of the as-grown microdisk laser on the Si substrate at 4.5 K (uncorrected from the cutoff of the filters after  $1.6 \mu\text{m}$ ). Inset: Surface morphology of single-layer InAs QDs on top of the InP-on-Si substrate; the color scale is 20 nm.

lasers by direct growth on the Si substrates would be highly advantageous.

In this Letter, we report for the first time  $1.55 \mu\text{m}$  band CW lasing of InAs/InAlGaAs quantum dot microdisk lasers epitaxially grown on (001) silicon. Previous lasers grown on silicon usually require special substrates such as patterning the silicon substrates<sup>17</sup> or adopting large offcut angles<sup>16</sup> that may hinder their wide applications in silicon photonics. Here, we are able to grow APD-free InP on standard (001) silicon wafers with slight unintentional miscuts ranging from  $0.3^\circ$  to  $0.8^\circ$ , showing an improved compatibility with CMOS technology and advantages in realizing better surface morphology. Another major challenge impeding the realization toward a  $1.55 \mu\text{m}$  QD laser on silicon is the InP-on-Si template growth. The large lattice mismatch ( $\sim 8\%$ ) between InP and Si gives rise to a high threading dislocation density (TDD) in the order of  $10^9$ – $10^{10}/\text{cm}^2$ , degrading device performances. In this work, we inserted seven layers of QDs into the InP-on-Si buffer as dislocation filters to reduce the TDD in the top InP layer to  $3.2 \times 10^8 \text{ cm}^{-2}$ . Although the three-dimensional QDs have been proven as effective dislocation filters in GaAs-on-Si due to their large strain fields,<sup>14</sup> this is the first application of InAs QDs in an InP-on-Si system to filter the TDs and allow high enough crystalline quality for laser growth. The dislocation filtering process has been recently reported in detail.<sup>23</sup> In addition, QDs

are also chosen as the active gain medium because they are less vulnerable to the dislocations engendered by lattice-mismatched growth, compared to their quantum well counterparts.<sup>19,24</sup> Nonradiative recombination can be reduced in the QD active region by greatly diluting the dislocations between the dense and discrete dots.<sup>25</sup> Compared with the InAs/GaAs QDs, the small lattice mismatch ( $\sim 3.2\%$ ) and complex strain distribution in InAs/InP introduce serious size and shape dispersions in QDs, leading to large inhomogeneous broadening.<sup>20</sup> We recently developed a double-capping procedure and strain-balancing technique to enhance optical performance and reduce QD inhomogeneity in the metal–organic chemical vapor deposition (MOCVD) growth of multilayer InAs/InAlGaAs QDs.<sup>26</sup> These techniques were applied in our microdisk laser growth. Moreover, microdisk structures with high-quality whispering-gallery modes (WGMs) and small mode volumes help minimize power consumption.<sup>27,28</sup> In this paper, we demonstrate a unique combination of these technologies to address some long-standing issues and achieve  $1.55 \mu\text{m}$  lasing from seven-layer QD microdisks at liquid-helium temperature with a threshold of 1.6 mW under continuous optical pumping.

Figure 1a illustrates the schematic of the epitaxial layers grown on a 4 in. (001) silicon substrate. The material growth was performed using an Aixtron AIX-200/4 MOCVD system.

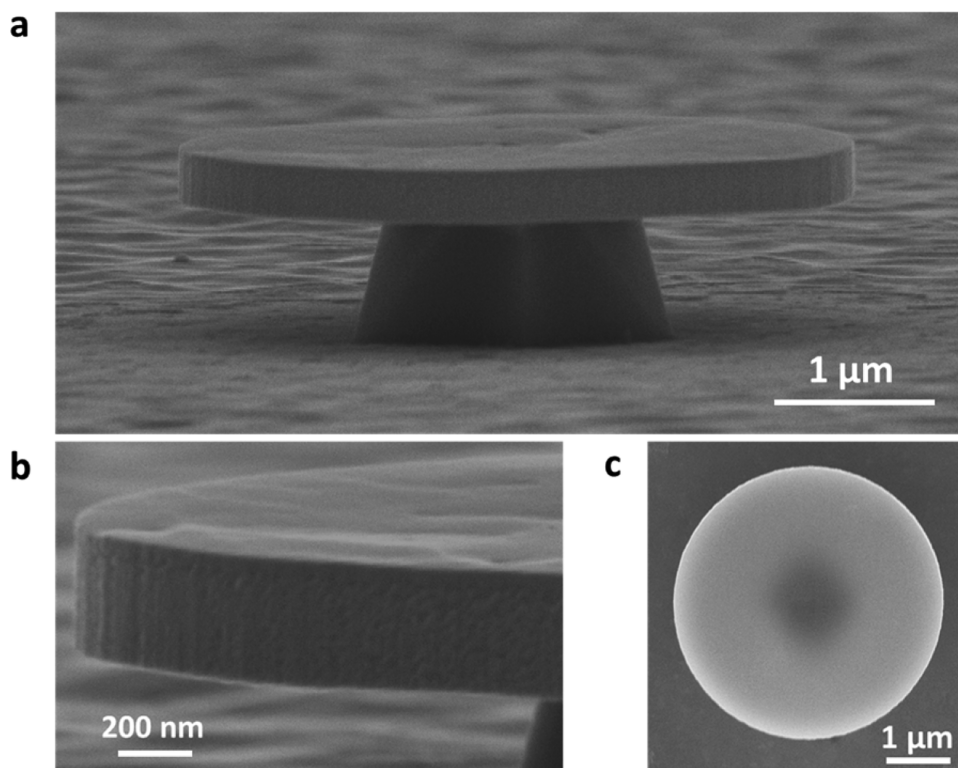


**Figure 2.** Scanning electron microscope image of a 4- $\mu\text{m}$ -diameter microdisk on Si. (a) Side view of the disk. (b) Close-up view of sidewall condition, indicating a steep vertical sidewall profile with slight roughness. (c) Top-down view of the disk, revealing a good circularity. The shadow in the center is related to the InP pedestal.

Beginning with a 500 nm GaAs intermediate buffer on Si, a 500 nm InP layer was subsequently grown by a two-step growth method.<sup>29</sup> Afterward, seven-stack InAs/InAlGaAs quantum dot dislocation filters were inserted,<sup>23</sup> followed by a 1  $\mu\text{m}$  InP buffer that will serve as the pillar of the microdisk lasers, to optically isolate the disk active region from the QD filters and the underlying Si substrate. The dislocation filtering function of the InAs/InAlGaAs QDs on the compliant InP-on-Si substrate is investigated by transmission electron microscopy (TEM), as shown in Figure 1b,c. It is noted that the TEM images presented here are slightly different from the real device structure in the exact insertion position of the QD dislocation filter, which we believe has minimal influence on dislocation filtering efficiency. From the large-area TEM in Figure 1b, only a few TDs can be noticed in the top InP layer. The full global-view TEM image can be seen in our recent publication.<sup>23</sup> Figure 1c illustrates the dislocations bent by the large strain field of the self-organized QDs. The bending effect enhances the probability of threading dislocation interaction and annihilation, resulting in a better quality of InP buffer above the QD dislocation filters.<sup>23</sup> The surface morphology of the InP-on-Si buffer was evaluated by atomic force microscopy (AFM), as depicted in Figure 1d. A surface that is free of APDs was obtained, with a root-mean-square (RMS) roughness of 3.1 nm across a scan area of  $5 \times 5 \mu\text{m}^2$ . This was attributed to the adjacent enough biatomic steps and suitable identical nucleation growth conditions to fully coalesce the antiphase boundaries formed in the early stage into a single-domain GaAs intermediate buffer.<sup>30</sup> The microdisk laser active structure consists of seven layers of QDs enclosed by symmetric 70-nm-thick  $\text{In}_{0.51}\text{Al}_{0.49}\text{As}$  cladding layers. The inset of Figure 1e presents the surface morphology of the uncapped InAs

quantum dots on the InP-on-Si template. The QD density is in the order of  $4 \times 10^{10} \text{ cm}^{-2}$ , with a few large InAs clusters appearing at the bumpy region of the InP-on-Si surface. Figure 1e displays the normalized power-dependent photoluminescence (PL) of the complete QD microdisk structure on Si at liquid-helium temperature (4.5 K). Ground-state emission at the  $\sim 1.55 \mu\text{m}$  telecom wavelength was observed with a broadband spectrum. The broad spectrum resulting from QD inhomogeneity allows for a better chance of overlap between resonant modes with a large free spectral range (FSR) and the material gain. With increased excitation power at 100  $\mu\text{W}$ , multipeaks started to appear on the top of the emission spectrum, attributed to monolayer fluctuations of the dot height.<sup>31</sup> The fwhm broadening with further excitation power increase was related with band-filling effects.

Microdisk lasers were fabricated using the colloidal lithography method.<sup>27,28</sup> The sample was predeposited with a thin layer of  $\text{SiO}_2$  before 4- $\mu\text{m}$ -diameter silica beads were dispersed onto the sample surface. The perfect round shape of the silica beads was then transferred to the  $\text{SiO}_2$  underlayer, forming hard masks for the subsequent disk dry-etch and pedestal wet-etch. It is noted that the emission spectra of microdisk lasers are quite sensitive to the disk sidewall condition, as well as the pillar undercut to form an air cladding structure. The different disk sidewalls formed in the dry-etch strongly affect scattering loss, while the nonuniformity in the undercut of the InP pillar during the wet-etch process will influence the optical losses for disk modes and affect the heat dissipation efficiency of the disks.<sup>32</sup> Figure 2a presents a cross-sectional scanning electron microscope (SEM) image of a microdisk laser, demonstrating the optically isolated structure. Figure 2b shows a close-up view of the disk sidewall, revealing a

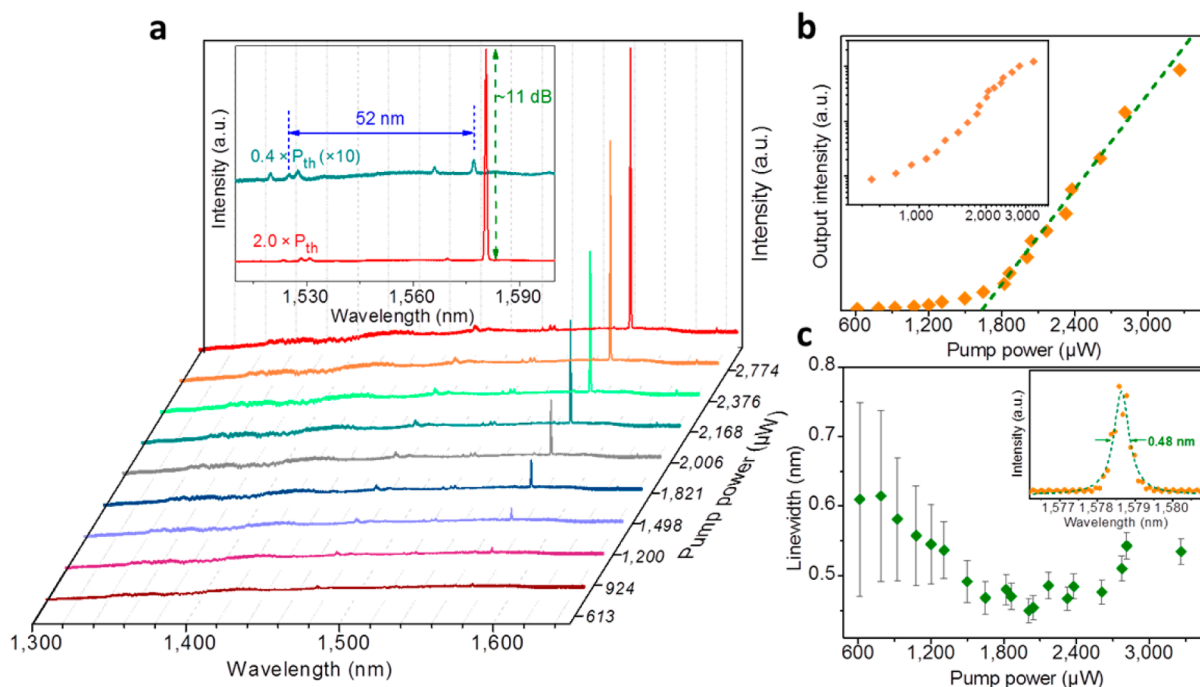


**Figure 3.** Lasing characteristics of a 4- $\mu\text{m}$ -diameter microdisk on Si. (a) Microphotoluminescence spectra as a function of pump power. Inset figure compares emission below and above threshold. (b) Linear plot of integrated output intensity versus effective input power (L–L curve), exhibiting a threshold of 1.6 mW for seven-layer QDs. The orange symbols represent the measured data, and the green dashed line is a linear fit to the L–L curve. Inset: Double-logarithmic plot of the L–L curve. (c) Line width evolution depending on the injection power. Inset: High-resolution spectrum at spontaneous emission (1.4 mW). The orange dots represent the measured data, which are fitted to a Lorentzian line shape, as shown by the green dashed line.

steep vertical profile. The slight roughness may be associated with the oxide hard mask sidewall erosion.<sup>33</sup> It is noted that QDs possess advantages in suppression of surface recombination at the disk sidewall,<sup>34</sup> minimizing the adverse effect of the microdisk sidewall roughness induced by the dry etching. The top-down view in Figure 2c indicates a good circular geometry of the microdisk region, which is favorable for the resonant modes. The dark shadow in the center is related to the anisotropic wet etching of the InP pedestal.<sup>35</sup> The lateral undercut resulting from the wet-etch was  $\sim 1.5 \mu\text{m}$ , providing a three-dimensional optical confinement of the air-cladded WGMs as well as a good thermal conductivity through the InP pillar.

The fabricated devices were characterized in a microphotoluminescence ( $\mu\text{-PL}$ ) system at 4.5 K, pumped by a CW 514 nm Ar ion laser. Figure 3a shows the power-dependent spectra emitted from the fabricated microdisk laser with a good device topology. Strong cavity mode modulation was observed as the pump power was raised, with a pronounced sharp peak at the telecom wavelength of 1.578  $\mu\text{m}$ . The spectra shown in the inset of Figure 3a demonstrate the weak mode modulation at low pump power ( $0.4 \times P_{\text{th}}$ ) and single-mode lasing at twice the threshold ( $2.0 \times P_{\text{th}}$ ). A high extinction ratio of  $\sim 11$  dB was achieved. The FSR of the first-order WGMs in this 4- $\mu\text{m}$ -diameter disk could be calculated using  $\Delta\lambda = \lambda^2 / 2\pi n_{\text{eff}} \approx 52 \text{ nm}$  ( $\lambda = 1.578 \mu\text{m}$ ), which agrees well with the observed spacing between the adjacent modes in the same radial order, as shown in the inset of Figure 3a. The single lasing mode at the maximum emission position of the as-grown PL spectrum (shown in Figure 1d) further verifies the efficient interaction of the QD gain medium with the WGM of the microdisk cavity. Figure 3b,c describe the output intensity (L–

L curve) and line width as a function of the effective pump power. The effective pumping power was estimated after taking multiple reflections/absorptions in the microdisk into consideration:  $(1 - R)[1 - \exp(-ad)] / [1 - R \times \exp(-ad)]$ .<sup>34</sup> In our case, the thickness of the disk,  $d$ , is  $\sim 0.45 \mu\text{m}$ , the average absorption coefficient of the disk region is on the order of  $\alpha \approx 10^5 \text{ cm}^{-1}$ , and the reflectivity at the microdisk surface is calculated to be  $R \approx 35\%$ , assuming a group refractive index of  $n = 3.8$ . Therefore, the effective threshold  $P_{\text{th}}$  was extrapolated to be  $\sim 1.6 \text{ mW}$  for the seven-layer QD active region. This was evidenced by a “kink” in the L–L curve, as shown in Figure 3b. The inset of Figure 3b plots the double logarithmic integrated photoluminescence intensity versus pump power, revealing a typical “S-shaped” nonlinear transition from spontaneous emission to amplified spontaneous emission up to lasing.<sup>36,37</sup> Figure 3c illustrates the line width narrowing as a function of the pumping power, further substantiating the lasing behavior. It is noted that there is a pronounced reduction of line width to 0.48 nm near the threshold. The cold cavity quality factor ( $Q$ ) for resonance can therefore be calculated with  $Q = \lambda_{\text{cav}} / \Delta\lambda_{\text{cav}}$ , where  $\lambda_{\text{cav}}$  is the peak wavelength of the resonant mode and  $\Delta\lambda_{\text{cav}}$  is the line width of the corresponding mode.<sup>28</sup> The  $Q$  factor was measured to be  $\sim 3289$  for the 4- $\mu\text{m}$ -diameter disk, which is among the highest reported  $Q$  values for microdisk lasers on InP substrates.<sup>32,38,39</sup> The slight line width increase when the pump power reaches twice the threshold power can be correlated to the chirping effects.<sup>37</sup> It is noted that temperature-dependent measurement of this microdisk laser is limited by the maximum power of the pumping laser source ( $\sim 5 \text{ mW}$ ). At liquid-nitrogen temperature (77 K), the lasing threshold has already surpassed the maximum pump power, and thus the lasing behavior was not observed.

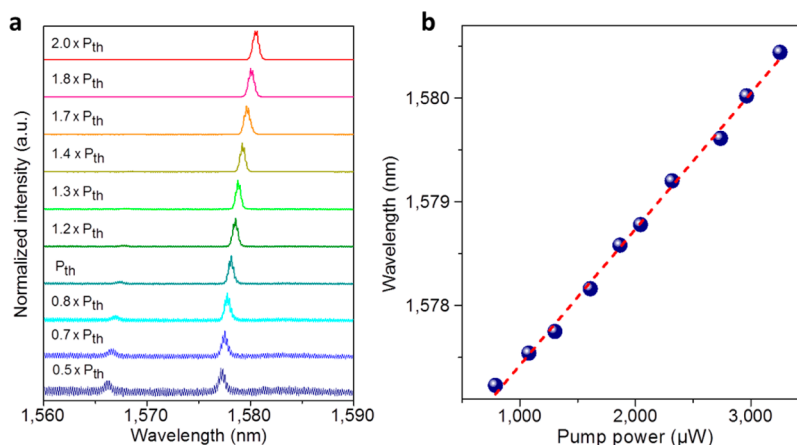


**Figure 4.** Power-dependent spectrum of a 4- $\mu\text{m}$ -diameter microdisk on Si. (a) Zoomed-in emission spectra taken at various pump powers, indicating a red-shift in wavelength as the pump power increases and mode competition toward single-mode lasing. (b) Peak wavelength of lasing mode as a function of pump power. The blue dots are the extracted peak wavelengths at different pump powers, linearly fitted by the red dashed line.

Figure 4a displays a red-shift of the emission peak induced by thermal effects as the pump power was ramped up. A red-shift rate of  $d\lambda/dP_{\text{pump}} = 1.3 \text{ nm/mW}$  was extracted through the linear fit, as plotted in Figure 4b. This evidences a small thermal impedance and sufficient heat dissipation.<sup>40</sup> Additionally, at the low excitation regime, two resonant modes could be detected from the zoomed-in power-dependent spectra in Figure 4a. As the excitation power increased beyond the threshold, all emission across the spectrum was enhanced, while the mode centered at  $\sim 1.578 \mu\text{m}$  dominated, indicating a transition from multimode spontaneous emission to single-mode lasing. The rapid dominance of the single mode contributes to the low thresholds of microdisk lasers.<sup>32,41,42</sup>

The successful realization of this 1.55  $\mu\text{m}$  band InP-based quantum dot laser on a Si (001) substrate can be attributed to the following two factors: One is the combination of InAs quantum dots as the gain medium with the microdisk topology, enabling a low-threshold, high-efficiency laser design. The other is the insertion of QDs into the InP-on-Si buffer serving as effective dislocation filters, generating a better crystalline quality of the active layers.

The next critical step toward room-temperature lasing on Si will involve further improvement of material quality for the InP buffer epitaxially grown on the Si (001) substrate by optimizing the number of the QD layers as dislocation filters. A lower dislocation density can directly lead to higher luminescence intensity and thus a better gain by the reduced nonradiative recombination, resulting in lower thresholds and a higher operation temperature. Fine-tuning of the QD layers will also enhance emission efficiency of the active region. Moreover, further improving the smoothness of disk sidewall will minimize light scattering.

In summary, we have demonstrated the first single-mode 1.55  $\mu\text{m}$  InAs/InAlGaAs/InP quantum dot microdisk laser monolithically grown on (001)-oriented planar Si substrates. Under continuous-wave optical pumping, strong laser emission at 1.578  $\mu\text{m}$  has been achieved with a low threshold of 1.6 mW at 4.5 K. This work thus provides a simple, straightforward, and potential low-cost path toward III–V long-wavelength lasers on silicon for on-chip optical interconnects.

## METHODS

**Growth of Quantum Dot Microdisk Laser on Si.** A standard 4-in. Si (001) substrate was first cleaned in  $\text{NH}_3\text{OH}/\text{H}_2\text{O}_2/\text{H}_2\text{O} = 1:1:5$  for 10 min and deoxidized by 1% HF etch for 1 min. Growth was subsequently performed in an AIX-200/4 horizontal MOCVD system. After 800  $^\circ\text{C}$  thermal cleaning for 15 min, the reactor was cooled to 390  $^\circ\text{C}$  with *tert*-butylarsine (TBA) introduced to grow a thin low-temperature (LT) GaAs nucleation layer ( $<10 \text{ nm}$ ). A 500 nm GaAs intermediate buffer was grown at three temperature windows: 550, 580, and 600  $^\circ\text{C}$ . The InP buffer was grown continuously: a  $\sim 65 \text{ nm}$  LT-InP seed layer at 430  $^\circ\text{C}$  and a  $\sim 500 \text{ nm}$  high-temperature (HT) InP buffer at 630  $^\circ\text{C}$  with a gradual increase of the growth rate from 3.5 nm/min to 30 nm/min. Seven-layer InAs/InAlGaAs QDs were deposited on top for dislocation filtering: A  $\sim 1.5 \text{ nm}$   $\text{In}_{0.4}\text{Ga}_{0.6}\text{As}$  wetting layer was grown first at 630  $^\circ\text{C}$  and then cooled down to 510  $^\circ\text{C}$  for QD growth. The QDs were grown for 10 s with a deposition amount of 3.6 monolayers and a V/III of  $\sim 0.4$ . After in situ annealing in TBA ambient for 5 s, a thin LT-InAlGaAs first cap layer ( $\sim 1.3 \text{ nm}$ ) was grown immediately at 510  $^\circ\text{C}$  for a fast capping of QDs as well as emission wavelength tuning. The reactor temperature was then increased to 630  $^\circ\text{C}$  in 5 min to grow another  $\sim 43 \text{ nm}$  HT-InAlGaAs second cap layer. This structure was repeated seven times to grow the seven-layer QDs. Once the dislocation filter has been completed, another 1- $\mu\text{m}$ -thick HT-InP buffer (functioning as the pedestal in the microdisk laser) was continued at 630  $^\circ\text{C}$ . Finally, the microdisk laser device was grown on top with the same seven-stack QD system embedded into two symmetric  $\sim 70 \text{ nm}$  HT- $\text{In}_{0.51}\text{Al}_{0.49}\text{As}$  cladding layers.

**Microdisk Laser Fabrication.** First of all, a 200 nm  $\text{SiO}_2$  thin film was deposited on the as-grown microdisk sample on the Si substrate by plasma-enhanced chemical vapor deposition as a hard mask for disk dry etching. Then a suspension filled with 4- $\mu\text{m}$ -diameter  $\text{SiO}_2$  microspheres (also called silica beads) was diluted in isopropyl alcohol (IPA) and dispersed onto the oxide surface by a micropipet. The sample was immediately placed onto a hot plate at 90  $^\circ\text{C}$  for a fast evaporation of IPA, leaving the microspheres for definition of the disk area. The perfectly round contour was then transferred to the 200 nm  $\text{SiO}_2$  hard mask by reactive-ion etching. Afterward, the spheres were removed by immersing the sample in acetone together with an ultrasonic bath. Inductively coupled

plasma (ICP) dry etching was performed subsequently to reach an etching depth of  $\sim 1.2 \mu\text{m}$ , terminating at the InP compliant substrate. The recipe of the ICP etching was based on a mixture of Ar and  $\text{BCl}_3$ , with flow rates of 20 and 4.5 sccm, respectively. Other key parameters include 500 W coil power and 100 W platen power, chamber pressure at 5 mTorr, an elevated substrate temperature of  $30^\circ\text{C}$  to help remove  $\text{In-Cl}_x$ , and a total etch time of 3 min. Afterward, a highly selective etchant ( $\text{HCl}/\text{H}_2\text{O} = 1:1$  for 90 s) was utilized to etch the remaining InP layer down to the seven-layer QD dislocation filter surface as well as laterally to form an undercut of  $\sim 1.5 \mu\text{m}$  for the InP pedestal. The optically isolated post structure can efficiently prevent WGMs on the periphery of the disk from coupling into the substrate and can also improve optical confinement in the vertical direction. Finally, the oxide hard mask was removed by buffered oxide etch.

**Laser Characterization.** Microphotoluminescence measurements were carried out at liquid-helium temperature (4.5 K) in a surface-normal pump/collection configuration, using a 514 nm CW Ar ion laser as the excitation source. The focused laser spot size was measured to be around  $3.5 \mu\text{m}$  in diameter and irradiated at the half center position of the fabricated sample surface by a  $50\times$ , 0.55 numerical aperture objective (MSPlan). Microdisk laser emission was detected by a thermoelectric-cooled InGaAs detector array. Filters were used to block excitation light from reaching any detectors. There is a cutoff of the filters after  $1.6 \mu\text{m}$ .

## AUTHOR INFORMATION

### Corresponding Author

\*Tel (K. M. Lau): (852) 23587049. Fax: (852) 23581485. E-mail: eekmlau@ust.hk.

### ORCID

Bei Shi: 0000-0003-3453-2358

### Author Contributions

K. M. Lau and E. L. Hu proposed and guided the overall project. Q. Li and B. Shi developed and performed material growth of InP-on-Si. B. Shi developed and performed material growth of quantum dots and microdisk laser epitaxial layers. B. Shi, S. Zhu, and Y. Wan developed and performed device fabrication and optical measurements. Q. Li and B. Shi performed TEM measurements. S. Zhu performed SEM measurements. B. Shi, S. Zhu, and K. M. Lau composed the manuscript. All authors assisted with the preparation of the manuscript and discussed the results.

### Notes

The authors declare no competing financial interest.

## ACKNOWLEDGMENTS

This work was supported in part by grants (Nos. 614813 and 16212115) from the Research Grants Council of Hong Kong. The authors would like to thank C. W. Tang for growth assistance, Prof. D. Bimberg, J.-H. Schulze, and D. Quandt for growth guidance, and the NFF and MCPF of HKUST for technical support. Helpful discussions with C. Liu and Y. Han are also acknowledged.

## REFERENCES

- (1) Zhou, Z.; Yin, B.; Michel, J. On-chip light sources for silicon photonics. *Light: Sci. Appl.* **2015**, *4*, e358.
- (2) Michel, J.; Liu, J.; Kimerling, L. C. High-performance Ge-on-Si photodetectors. *Nat. Photonics* **2010**, *4*, 527–534.

- (3) Reed, G. T.; Mashanovich, G.; Gardes, F. Y.; Thomson, D. J. Silicon optical modulators. *Nat. Photonics* **2010**, *4*, 518–526.

- (4) Xia, F.; Sekaric, L.; Vlasov, Y. Ultracompact optical buffers on a silicon chip. *Nat. Photonics* **2007**, *1*, 65–71.

- (5) Chaisakul, P.; Marris-Morini, D.; Frigerio, J.; Chrastina, D.; Rouified, M.; Cecchi, S.; Crozat, P.; Isella, G.; Vivien, L. Integrated germanium optical interconnects on silicon substrates. *Nat. Photonics* **2014**, *8*, 482–488.

- (6) Liang, D.; Bowers, J. E. Recent progress in lasers on silicon. *Nat. Photonics* **2010**, *4*, 511–517.

- (7) Liu, J.; Sun, X.; Camacho-Aguilera, R.; Kimerling, L. C.; Michel, J. Ge-on-Si laser operating at room temperature. *Opt. Lett.* **2010**, *35*, 679–681.

- (8) Justice, J.; Bower, C.; Meitl, M.; Mooney, M. B.; Gubbins, M. A.; Corbett, B. Wafer-scale integration of group III–V lasers on silicon using transfer printing of epitaxial layers. *Nat. Photonics* **2012**, *6*, 612–616.

- (9) Fang, A. W.; Park, H.; Cohen, O.; Jones, R.; Paniccia, M.; Bowers, J. E. Electrically pumped hybrid AlGaInAs-silicon evanescent laser. *Opt. Express* **2006**, *14*, 9203–9210.

- (10) Tanabe, K.; Watanabe, K.; Arakawa, Y. III-V/Si hybrid photonic devices by direct fusion bonding. *Sci. Rep.* **2012**, *2*, 349.

- (11) Van Campenhout, J.; Rojo-Romeo, P.; Regreny, P.; Seassal, C.; Van Thourhout, D.; Verstuyft, S.; Di Cioccio, L.; Fedeli, J.; Lagahe, C.; Baets, R. Electrically pumped InP-based microdisk lasers integrated with a nanophotonic silicon-on-insulator waveguide circuit. *Opt. Express* **2007**, *15*, 6744–6749.

- (12) Jhang, Y.-H.; Tanabe, K.; Iwamoto, S.; Arakawa, Y. InAs/GaAs quantum dot lasers on silicon-on-insulator substrates by metal-stripe wafer bonding. *IEEE Photonics Technol. Lett.* **2015**, *27*, 875–878.

- (13) Shi, B.; Li, Q.; Wan, Y.; Ng, K. W.; Zou, X.; Tang, C. W.; Lau, K. M. InAlGaAs/InAlAs MQWs on Si Substrate. *IEEE Photonics Technol. Lett.* **2015**, *27*, 748–751.

- (14) Yang, J.; Bhattacharya, P.; Mi, Z. High-performance  $\text{In}_{0.5}\text{Ga}_{0.5}\text{As}/\text{GaAs}$  quantum-dot lasers on silicon with multiple-layer quantum-dot dislocation filters. *IEEE Trans. Electron Devices* **2007**, *54*, 2849–2855.

- (15) Wang, T.; Liu, H.; Lee, A.; Pozzi, F.; Seeds, A.  $1.3\text{-}\mu\text{m}$  InAs/GaAs quantum-dot lasers monolithically grown on Si substrates. *Opt. Express* **2011**, *19*, 11381–11386.

- (16) Liu, A. Y.; Zhang, C.; Norman, J.; Snyder, A.; Lubyshev, D.; Fastenau, J. M.; Liu, A. W. K.; Gossard, A. C.; Bowers, J. E. High performance continuous wave  $1.3 \mu\text{m}$  quantum dot lasers on silicon. *Appl. Phys. Lett.* **2014**, *104*, 041104.

- (17) Wan, Y.; Li, Q.; Liu, A. Y.; Gossard, A. C.; Bowers, J. E.; Hu, E. L.; Lau, K. M. Optically pumped  $1.3 \mu\text{m}$  room-temperature InAs quantum-dot micro-disk lasers directly grown on (001) silicon. *Opt. Lett.* **2016**, *41*, 1664–1667.

- (18) Liu, A. Y.; Herrick, R. W.; Ueda, O.; Petroff, P. M.; Gossard, A. C.; Bowers, J. E. Reliability of InAs/GaAs quantum dot lasers epitaxially grown on silicon. *IEEE J. Sel. Top. Quantum Electron.* **2015**, *21*, 1900708.

- (19) Chen, S.; Li, W.; Wu, J.; Jiang, Q.; Tang, M.; Shutts, S.; Elliott, S. N.; Sobiesierski, A.; Seeds, A. J.; Ross, I.; Smowton, P. M.; Liu, H. Electrically pumped continuous-wave III-V quantum dot lasers on silicon. *Nat. Photonics* **2016**, *10*, 307–311.

- (20) Khan, M. Z. M.; Ng, T. K.; Ooi, B. S. Self-assembled InAs/InP quantum dots and quantum dashes: Material structures and devices. *Prog. Quantum Electron.* **2014**, *38*, 237–313.

- (21) Cerutti, L.; Rodriguez, J. B.; Tournie, E. GaSb-based laser, monolithically grown on silicon substrate, emitting at  $1.55 \mu\text{m}$  at room temperature. *IEEE Photonics Technol. Lett.* **2010**, *22*, 553–555.

- (22) Bhowmick, S.; Baten, M. Z.; Frost, T.; Ooi, B. S.; Bhattacharya, P. High performance InAs/ $\text{In}_{0.53}\text{Al}_{0.23}\text{Ga}_{0.24}\text{As}/\text{InP}$  quantum dot  $1.55 \mu\text{m}$  tunnel injection laser. *IEEE J. Quantum Electron.* **2014**, *50*, 7–14.

- (23) Shi, B.; Li, Q.; Lau, K. M. Self-organized InAs/InAlGaAs quantum dots as dislocation filters for InP films on (001) Si. *J. Cryst. Growth* **2016**, DOI: 10.1016/j.jcrysgro.2016.10.089.

(24) Liu, H.; Wang, T.; Jiang, Q.; Hogg, R.; Tutu, F.; Pozzi, F.; Seeds, A. Long-wavelength InAs/GaAs quantum-dot laser diode monolithically grown on Ge substrate. *Nat. Photonics* **2011**, *5*, 416–419.

(25) Liu, A. Y.; Srinivasan, S.; Norman, J.; Gossard, A.; Bowers, J. E. Quantum dot lasers for silicon photonics. *Photonics Res.* **2015**, *3*, B1–B9.

(26) Shi, B.; Lau, K. M. Enhanced optical properties of InAs/InAlGaAs/InP quantum dots grown by metal-organic chemical vapor deposition using a double-cap technique. *J. Cryst. Growth* **2016**, *433*, 19–23.

(27) Aharonovich, I.; Woolf, A.; Russell, K. J.; Zhu, T.; Niu, N.; Kappers, M. J.; Oliver, R. A.; Hu, E. L. Low threshold, room-temperature microdisk lasers in the blue spectral range. *Appl. Phys. Lett.* **2013**, *103*, 021112.

(28) Tamboli, A. C.; Haberer, E. D.; Sharma, R.; Lee, K.; Nakamura, S.; Hu, E. L. Room-temperature continuous-wave lasing in GaN/InGaN microdisks. *Nat. Photonics* **2007**, *1*, 61–64.

(29) Li, Q.; Tang, C. W.; Lau, K. M. Growth of ultra-high mobility In<sub>0.52</sub>Al<sub>0.48</sub>As/In<sub>x</sub>Ga<sub>1-x</sub>As (x ≥ 53%) quantum wells on Si substrates using InP/GaAs buffers by metalorganic chemical vapor deposition. *Appl. Phys. Express* **2014**, *7*, 045502.

(30) Bogumilowicz, Y.; Hartmann, J. M.; Cipro, R.; Alcotte, R.; Martin, M.; Bassani, F.; Moeyaert, J.; Baron, T.; Pin, J. B.; Bao, X.; Ye, Z.; Sanchez, E. Anti-phase boundaries—Free GaAs epilayers on ‘quasi-nominal’ Ge-buffered silicon substrates. *Appl. Phys. Lett.* **2015**, *107*, 212105.

(31) Brault, J.; Gendry, M.; Grenet, G.; Hollinger, G.; Desieres, Y.; Benyattou, T. Alloying effects in self-assembled InAs/InP dots. *J. Cryst. Growth* **1999**, *201*, 1176–1179.

(32) McCall, S. L.; Levi, A. F. J.; Slusher, R. E.; Pearton, S. J.; Logan, R. A. Whispering-gallery mode microdisk lasers. *Appl. Phys. Lett.* **1992**, *60*, 289–291.

(33) Choi, S. J.; Djordjev, K.; Choi, S.; Dapkus, P. D. CH<sub>4</sub>-based dry etching of high Q InP microdisks. *J. Vac. Sci. Technol., B: Microelectron. Process. Phenom.* **2002**, *20*, 301–305.

(34) Ide, T.; Baba, T.; Tatebayashi, J.; Iwamoto, S.; Nakaoka, T.; Arakawa, Y. Room temperature continuous wave lasing in InAs quantum-dot microdisks with air cladding. *Opt. Express* **2005**, *13*, 1615–1620.

(35) Chu, D. Y.; Chin, M. K.; Sauer, N. J.; Xu, Z.; Chang, T. Y.; Ho, S. T. 1.5 μm InGaAs/InAlGaAs Quantum-Well Microdisk Lasers. *IEEE Photonics Technol. Lett.* **1993**, *5*, 1353.

(36) Wang, Z.; Tian, B.; Pantouvaki, M.; Guo, W.; Absil, P.; Van Campenhout, J.; Merckling, C.; Van Thourhout, D. Room-temperature InP distributed feedback laser array directly grown on silicon. *Nat. Photonics* **2015**, *9*, 837–842.

(37) Tatebayashi, J.; Kako, S.; Ho, J.; Ota, Y.; Iwamoto, S.; Arakawa, Y. Room-temperature lasing in a single nanowire with quantum dots. *Nat. Photonics* **2015**, *9*, 501–505.

(38) Slusher, R. E.; Levi, A. F. J.; Mohideen, U.; McCall, S. L.; Pearton, S. J.; Logan, R. A. Threshold characteristics of semiconductor microdisk lasers. *Appl. Phys. Lett.* **1993**, *63*, 1310–1312.

(39) Seassal, C.; Letartre, X.; Brault, J.; Gendry, M.; Pottier, P.; Viktorovitch, P.; Piquet, O.; Blondy, P.; Cros, D.; Marty, O. InAs quantum wires in InP-based microdisks: Mode identification and continuous wave room temperature laser operation. *J. Appl. Phys.* **2000**, *88*, 6170–6174.

(40) Kryzhanovskaya, N. V.; Zhukov, A. E.; Maximov, M. V.; Moiseev, E. I.; Shostak, I. I.; Nadtochiy, A. M.; Kudashova, Y. V.; Lipovskii, A. A.; Kulagina, M. M.; Troshkov, S. I. Room temperature lasing in 1-μm microdisk quantum dot lasers. *IEEE J. Sel. Top. Quantum Electron.* **2015**, *21*, 1900905.

(41) Sandoghdar, V.; Treussart, F.; Hare, J.; Seguin, L.; Raimond, J. M.; Haroche, S. Very low threshold whispering-gallery-mode microsphere laser. *Phys. Rev. A: At., Mol., Opt. Phys.* **1996**, *54*, R1777.

(42) Wan, Y.; Li, Q.; Liu, A. Y.; Gossard, A. C.; Bowers, J. E.; Hu, E. L.; Lau, K. M. Sub-wavelength InAs quantum dot micro-disk lasers epitaxially grown on exact Si (001) substrates. *Appl. Phys. Lett.* **2016**, *108*, 221101.